Nat. Hazards Earth Syst. Sci., 23, 2663–2681, 2023
https://doi.org/10.5194/nhess-23-2663-2023

Natural Hazards and Earth System Sciences
Open Access
EGU

An integrated modeling approach to evaluate the impacts of nature-based solutions of flood mitigation across a small watershed in the southeast United States

Betina I. Guido[1], Ioana Popescu[1], Vidya Samadi[2], and Biswa Bhattacharya[1]

[1]Department of Hydroinformatics and Socio-Technical Innovation, IHE Delft Institute for Water Education, Delft, 2611 AX, the Netherlands
[2]Department of Agricultural Sciences, Clemson University, Clemson, SC 29634, United States of America

Correspondence: Betina I. Guido (betinaguido@gmail.com)

Received: 6 December 2022 – Discussion started: 5 January 2023
Revised: 24 May 2023 – Accepted: 14 June 2023 – Published: 28 July 2023

Abstract. Floods are among the most destructive natural hazards in the world, posing numerous risks to societies and economies globally. Accurately understanding and modeling floods driven by extreme rainfall events has long been a challenging task in the domains of hydrologic science and engineering. Unusual catchment responses to flooding cause great difficulty in predicting the variability and magnitude of floods, as well as proposing solutions to manage large volumes of overland flow. The usage of nature-based solutions (NBSs) has proved to be effective in the mitigation of flood peak rate and volume in urban or coastal areas, yet it is still not widely implemented due to limited knowledge and testing compared to traditional engineering solutions. This research examined an integrated hydrological and hydraulic modeling system to understand the response of an at-risk watershed system to flooding and evaluate the efficacy of NBS measures. Using the Hydrologic Engineering Center Hydrologic Modeling System and River Analysis System (HEC-HMS and HEC-RAS) software, an integrated hydrologic–hydraulic model was developed for Hurricane Matthew- (2016) and Florence-driven (2018) floods across the Little Pee Dee–Lumber River watershed, North and South Carolina (the Carolinas), US. The focus was on Nichols, a small town that has disproportionately been impacted by flooding during these two hurricane events.

The present article proposes a methodology for selecting, modeling, and evaluating the performance of NBS measures within a catchment, which can be extended to other case studies. Different NBS measures, including flood storage ponds, riparian reforestation, and afforestation in croplands, were designed, modeled, and evaluated. Hurricane Matthew's flooding event was used for evaluating the NBS scenarios given its high simulation accuracy in flood inundation compared to the less accurate results obtained for Hurricane Florence. The scenario comparison evidenced that large-scale natural interventions, such as afforestation in croplands, can reduce the inundated area in Nichols by 8 % to 18 %. On the contrary, the smaller-scale interventions such as riparian reforestation and flood storage ponds showed a negligible effect of only 1 % on flood mitigation.

1 Introduction

Floods are among the most destructive natural hazards in the world, posing numerous risks to societies and economies globally (European Parliament, 2017; IPCC, 2022). The socioeconomic impacts of flooding are numerous, negatively affecting human life, health, livelihoods, and critical infrastructure, among others (Phillips et al., 2018; IPCC, 2022).

In the United States, flooding and severe storms are among the most recurrent weather and climate disasters, which have caused USD 492 billion in economic damages in the past 30 years (Smith, 2020). The US Gulf and East Coast are vulnerable to destructive tropical storms and hurricanes, which can generate storm surges and riverine flooding along the exposed communities (NOAA, 2020). Since the 1970s inland flooding has been responsible for more than half of all deaths associated with tropical cyclones in the United States

(NOAA, 2018). The state of South Carolina (SC) alone has suffered almost USD 7 billion in flood and hurricane damages in the last 25 years (SCDNR, 2020). This state was recently overwhelmed by the impacts of five hurricanes in a time span of only 7 years, which generated severe riverine floods across cities and towns (Williams et al., 2019). According to the Intergovernmental Panel on Climate Change (IPCC) reports (e.g., IPCC, 2022), there will be an increase in the tropical cyclone rainfall intensities, as well as in the proportion that reaches very intense levels (Category 4 and 5) as a result of climate change (Knutson, 2022; Stone and Cohen, 2017). In addition, it is expected that global warming would also reduce the speed of tropical cyclones, resulting in more precipitation falling over a longer period, thus increasing flooding hazards (Kossin, 2018).

On top of the climatic causes of riverine flooding, it is expected that the future development of floodplains will raise the number of houses and citizens at risk in SC (SCDNR, 2020). Many of the new constructions of the last decade in the state were built in proximity to permanent water bodies (Tedesco et al., 2020). In SC, wetlands and forests have experienced significant losses since historic dates (Fish and Dahl, 1999). There are several indications that the loss of these ecosystems along with a growth in urbanization are key drivers of increasing flood peaks and volumes in rivers and floodplains (Bronstert et al., 2002).

Systematic efforts within the research community have been made to simulate hurricane-driven floods (Chen et al., 2021; Wing et al., 2019; among others). Accurate flood prediction and inundation mapping are vital for improving forecasts and resiliency, as well as reducing economic damages caused by extreme events (Grimaldi et al., 2019). However, understanding and accurately predicting major floods driven by hurricanes have long been a challenge in the fields of hydrologic science and engineering (Phillips et al., 2018; NOAA, 2018; Wing et al., 2019). The spatiotemporal variability of hurricane events, rapid and unusual catchment responses to flooding, and various sources of model errors make accurate flood modeling a challenging task (Teng et al., 2017; El Gharamti et al., 2021; Zhou et al., 2021). Numerous improvements have been developed for increased accuracy in flood inundation modeling and mapping over the years (Abbott et al., 1986; Dutta et al., 2006, 2013). Among others, remote sensing technologies have gained popularity in recent years, which are mainly used as an aid for flood simulation and mapping to validate and calibrate hydrological and hydraulic models (Chen et al., 2021; Teng et al., 2017).

Given the complexity of flood prediction and the increased flood hazard due to regional and global changes, an integrated physics-based flood model would overcome barriers in designing appropriate modeling architectures to represent rainfall–flooding processes. Hydrologic and hydraulic modeling integration has the benefit of using up-to-date software to model the dynamics of extreme events (Anselmo et al., 1996). This implies using a range of atmospheric, hydrologic, and hydraulic data and encompassing several processes across the water cycle. This research explores how to represent these complex processes in an integrated physics-based fashion to accurately reproduce past hurricane-driven floods.

The present research focuses on a small watershed, the Little Pee Dee (LPD) and Lumber River watershed, affluents to the Pee Dee River in eastern North and South Carolina (the Carolinas). Nichols, located at the confluence of the Little Pee Dee and Lumberton rivers, is one of the most severely impacted regions in this watershed. The town was devastated by Hurricane Matthew in October 2016, and, while the residents were still recovering, Hurricane Florence ravaged the community once more in September 2018 (Edwards, 2020; Stewart and Berg, 2019). Despite the widespread devastation in the area, it is unlikely that any flood protection measures will be implemented in the short term, since no advanced studies of the river's hydrodynamic behavior have been conducted so far. In light of this, there is an undeniable need for flood research that can provide insights into extreme hazard and flood risk management to protect the region from current and future damage.

Previous research has evaluated grey engineering flood mitigation measures such as levees and the elevation of bridges to protect Nichols (Muller, 2020). Although these traditional engineering measures are widely evaluated and can significantly reduce local flood hazards, they are often categorized as an expensive and inflexible approach (Brink et al., 2016). Nature-based solutions (NBSs), on the contrary, have been gaining popularity in the past few years, given their capacity to mitigate flood hazards and improve resilience in cost-effective ways (Cohen-Shacham et al., 2016; EESI, 2019; Ruangpan et al., 2020). In an area strongly affected by climatic disasters, which are expected to increase due to climate change and urbanization, it is crucial to explore a more nature-based approach that can adapt to future alterations and provide benefits at a watershed level (Kalantari et al., 2018).

NBSs can decrease and/or delay floodwater peaks and volumes using natural processes, reduce the magnitude of riverine floods, and increase the lead time to give more time for emergency response (Lama et al., 2021). The International Union for Conservation of Nature (IUCN), the World Bank Group, and the World Resources Institute (WRI) define NBSs as "actions to protect, sustainably manage, and restore natural and modified ecosystems that address societal challenges effectively and adaptively, simultaneously providing human well-being and biodiversity benefits" (IUCN, 2022). Such solutions can improve flood risk, combat climate change, improve water quality, restore and protect wetlands, stabilize shorelines, and reduce urban heat island effects, among others (European Commission, 2022). The use of these kinds of solutions in an area where nature is one of its main attractions such as Nichols is imperative.

Even though the concept of NBSs is well known, NBS incorporation into hydrologic and hydraulic models is not yet well understood and explored in the hydrology community (Kumar et al., 2021; Sahani, et al., 2019). To address this problem, this research determines a methodology for selecting, modeling, and evaluating the performance of NBSs and improving the theoretical as well as modeling aspects of NBS implementation.

The research paper is structured as follows. The case study is presented in Sect. 2. Section 3 introduces the methodology, including the models, NBS scenarios, and performance metrics. The subsequent sections summarize the results of the models, discussions, and conclusions.

2 Study case and data collection

The study area, covering 7000 km^2, is the LPD and Lumber River watershed, forming part of the lower Pee Dee River basin located in the Carolinas, US (Fig. 1). These rivers originate in North Carolina's Sandhills area and run south and east to SC's lower Coastal Plain (Howie, 2020). From its headwaters, the Lumber River takes its course of 185 km before merging with the LPD River shortly after entering SC (SCDNR, 2009). Downstream of the confluence, the river continues with the name of LPD River, until it discharges into the Pee Dee River. The LPD River has a length of 140 km from its origin to the watershed outlet. The outlet was defined at the Galivants Ferry bridge a few kilometers downstream of Nichols and the LPD–Lumber River intersections. At the river's intersection, the Lumber and LPD watersheds have an area of 4500 and 2000 km^2, respectively. At Galivants Ferry, the annual average discharge is about 78 $m^3\,s^{-1}$ with a maximum recorded discharge value of 1832 $m^3\,s^{-1}$, which occurred on 21 September 2018 (USGS, 2023).

In the eastern portions of SC and the Coastal Plain, the annual average rainfall ranges from 1143 to 1320 mm. Most years, during summer and early fall, SC is affected by tropical storms or hurricanes (DNR, 2021). Hurricanes Matthew and Florence were the latest to create significant flooding in the watershed that was selected for this study.

High terrain elevations can be observed at the origins of the Lumber and LPD rivers, reaching up to 225 m above sea level. However, in the rest of the area, the elevation is low with gentle gradients. The National Elevation Dataset (NED) of the USGS was retrieved and incorporated as terrain data into the models. The terrain elevation data with a resolution of 30×30 m and 10×10 m were used for hydrological and hydraulic modeling, respectively. All elevation values are in meters and are referenced to the North American Vertical Datum of 1988 (NAVD 88).

The land cover of the watershed is dominated by woody wetlands (32 %), followed by agriculture (31 %), forests (18 %), developed areas (10 %), grasslands and shrubs (6 %), emergent herbaceous wetlands (2 %), and open water (1 %). The Land Use Land Cover (LULC) map is shown in Fig. 2. The wetland and forest ecosystems have experienced high losses since historic dates, with notorious increases in farmland and residential areas. In the past 20 years, the major LULC changes have been caused by deforestation in woody wetlands and forests. The predominant hydrological soil groups in the watershed are A/D, B/D, and C/D, indicating slow infiltration rates in undrained areas. All these characteristics, gentle slope, dense vegetation, low-relief river, and poorly drained soils, make the area prone to surface ponding with long residence times.

According to the information retrieved from the National Inventory of Dams (NID), the watershed is covered by storage areas such as reservoirs, lakes, and dams, which can store water volumes during extreme rainfall events (see Fig. 2). However, even in the presence of these topographic terraces, reservoirs, and wetlands, the current storage capacity in the watershed is not enough to avoid destructive flooding events derived from severe storms, like those that occurred during hurricanes Matthew and Florence.

Local datasets are available from different US institutions, which were used as inputs for the proposed hydrologic and hydraulic models. Table 1 summarizes the data used in this research along with their corresponding sources and resolutions.

The precipitation data were collected from NOAA and USGS, which have different spatial and temporal resolutions. For hurricanes Matthew and Florence, the average total precipitation in the watershed according to the NOAA dataset was 287 and 388 mm, respectively. The spatial distribution of the rainfall was investigated using inverse distance weighted (IDW) and kriging methods. The IDW estimates values for unsampled points by the weighted average of observed data at surrounding stations. It relies on the theory that the unknown value of a point is more influenced by closer points than by points further away. Ordinary kriging is a geostatistical interpolation method based on a Gaussian process that considers the spatial variance of the precipitation. The method optimizes the station weights using probability functions, and these weights are used to interpolate values for unsampled points across the spatial field (Ly et al., 2011). Interpolation results revealed that cumulative precipitation values during Hurricane Florence were higher in the east of the watershed, whereas for Matthew the maximum volumes appeared in the south.

The streamflow and river stage data are compiled from the National Water Information System of USGS. There are eight streamflow stations with up-to-date data inside the watershed. The newest station was installed next to Nichols in 2017, after Hurricane Matthew's occurrence. Among all gauges, the Galivants Ferry station, located at the outlet of the watershed, has the most prolonged period of data, with records starting from 1986 to the present. The data show that the two most extreme flood events of the past 35 years occurred only in the last 5 years. These events were hurricanes

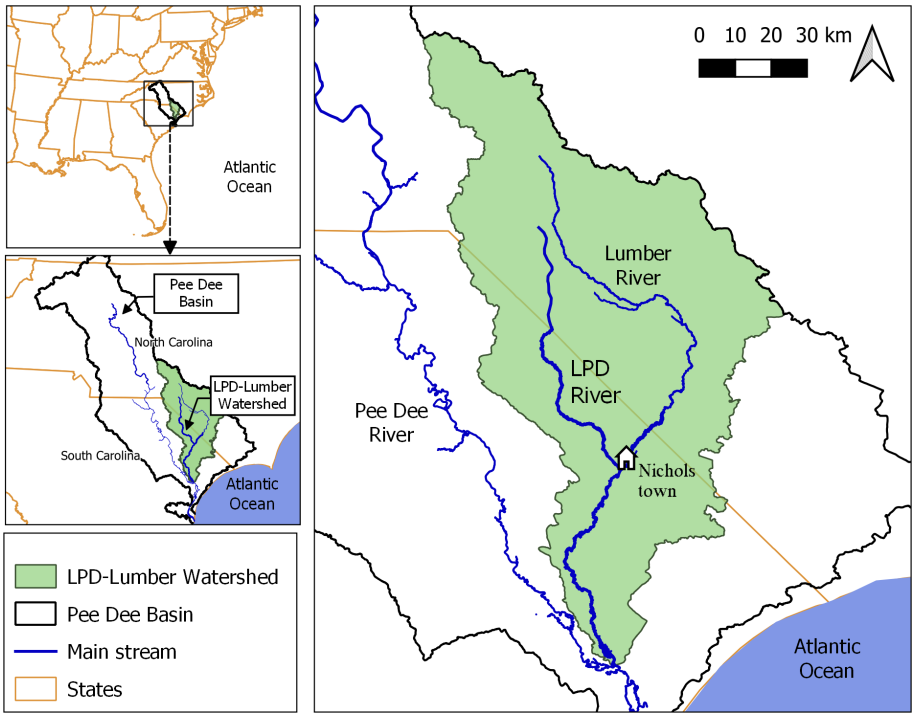

Figure 1. LPD and Lumber River watershed location.

Table 1. List of data used in the study.

Data type	Spatial resolution	Time resolution	Source	Usage
DEM	30 × 30 m 10 × 10 m	–	National Elevation Dataset (NED) by USGS	Hydrological and hydraulic simulations
Gauge rainfall	12 stations four stations	24 h 15 min	NOAA USGS	Hydrological simulation
Streamflow and water depth gauges	Eight stations	15 min	USGS	Hydrological simulation
LULC	30 m	–	MRLC consortium	Hydrological and hydraulic simulations
Soils	1 km	–	Web Soil Survey by USDA-NRCS	Hydrological simulation
Satellite-based flood inundation extent	250 m	–	Dartmouth Flood Observatory	Hydraulic simulation

Matthew and Florence, reaching peak discharges of 1679 and 1832 $m^3 s^{-1}$, respectively.

Table 2 exhibits information about the USGS stations' metadata (site number, location, contributing area, and peak discharge) during the last major hurricane events. The rainfall and streamflow gauge locations are presented in Fig. 4.

The observed flood inundation area was retrieved from remote sensing data. We used Dartmouth Flood Observatory of Colorado University inundation data for hurricanes Matthew and Florence. The inundation images are from MODIS 250 m, and Landsat 8 data were downloaded as raster and converted to flood extent maps. Hurricane Matthew's inundation images were validated by the Dartmouth Flood Observatory with Google Satellite images.

3 Methodology

To simulate the flooding processes and assess the performance of NBSs in the LPD–Lumberton watershed, an integrated hydrological–hydraulic model was developed using

Table 2. Peak discharge during hurricanes Florence and Matthew at eight USGS gauging stations (USGS, 2023).

USGS site no.	USGS site location	Contributing area (km^2)	Peak discharge ($m^3\ s^{-1}$, dd/mm/yyyy)			
			Hurricane Florence		Hurricane Matthew	
02135000	Galivants Ferry	7226	1832	21/09/2018	1679	12/10/2016
02134900	Nichols	4325	1175	20/09/2018	No records	–
02134500	Boardman	3181	1002	18/09/2018	1082	11/10/2016
02134170	Lumberton	1834	484	17/09/2018	413	10/10/2016
02133624	Maxton	945	348	17/09/2018	192	11/10/2016
02133500	Hoffman	474	283	19/09/2018	159	09/10/2016
02134480	Tar Heel	593	377	17/09/2018	549	10/10/2016
02132320	Laurinburg	216	172	17/09/2018	42	09/10/2016

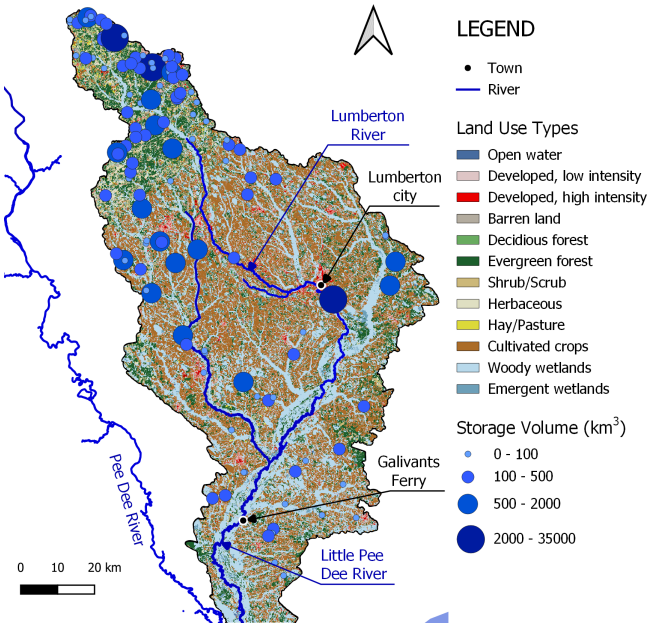

Figure 2. LULC map and storage areas.

the US Army Corps of Engineering software, i.e., the Hydrologic Engineering Center Hydrologic Modeling System (HEC-HMS) and River Analysis System (HEC-RAS). Simulations of hurricanes Matthew and Florence, two of the most damaging flood events in the LPD–Lumber watershed in the past few years, were developed and used as case studies for this research. The HEC software has widely been used to assess flood hazards in various US catchments (Bhusal et al., 2022; Knebl et al., 2005; Tang et al., 2020).

Figure 3 shows the modeling workflow followed in this study to develop an integrated hydrologic–hydraulic modeling system and assess the current situation in the watershed for NBS implementation. The first step was the data collection and pre-processing. We then developed a hydrological model to calibrate hurricane-driven flooding events. The simulated hydrograph was then used as a boundary condition for flood inundation mapping using the HEC-RAS model.

Finally, NBS scenarios were designed and implemented in the models, and steps 2 and 3 were repeated with the required adjustments. Depending on the selected NBS, finer DEM might be required. Such is the example of sand traps in a river. The tested solutions in this case study were related to LULC and buffer strips along the river, which were suitable for the DEM resolution of the models used, i.e., 30×30 m for the HEC-HMS model, and cross sections in the HEC-RAS model based on a 10×10 m DEM of the channel. New flood maps were obtained and compared with the baseline scenario to evaluate the performance of NBSs on flood mitigation at Nichols.

3.1 Hydrological modeling

Using HEC-HMS, a hydrological semi-distributed model for the LPD and Lumber River watersheds was developed, where each sub-basin is represented as a lumped model. With version HEC-HMS 4.9, the sub-basins and reaches were automatically delineated, using $30\ m \times 30\ m$ DEM data. In total, the watershed was divided into 10 sub-basins with eight of them including a USGS flood gauge at the outlet. The delineated sub-basins, reaches, and flood gauges are shown in Fig. 4.

The Soil Conservation Service (SCS) curve number (CN) method was chosen to simulate the precipitation loss, the Clark unit hydrograph (CUH) was chosen as the transformation method, and an exponential recession was chosen to model the baseflow (US Army Corps of Engineers, 2021).

The SCS CN method is used for event-based simulation and has extensively been used for US catchments. This approach has successfully been used in 2018 by the North Carolina Emergency Management agency to simulate the hydrological behavior of Hurricane Matthew in the Lumber River (Emergency Management NC, 2018).

The model estimates the runoff as the precipitation excess, which is derived from the cumulative precipitation and precipitation loss. The latter is estimated based on soils, lithology, land cover, and land use data (US Army Corps of Engineers, 2021).

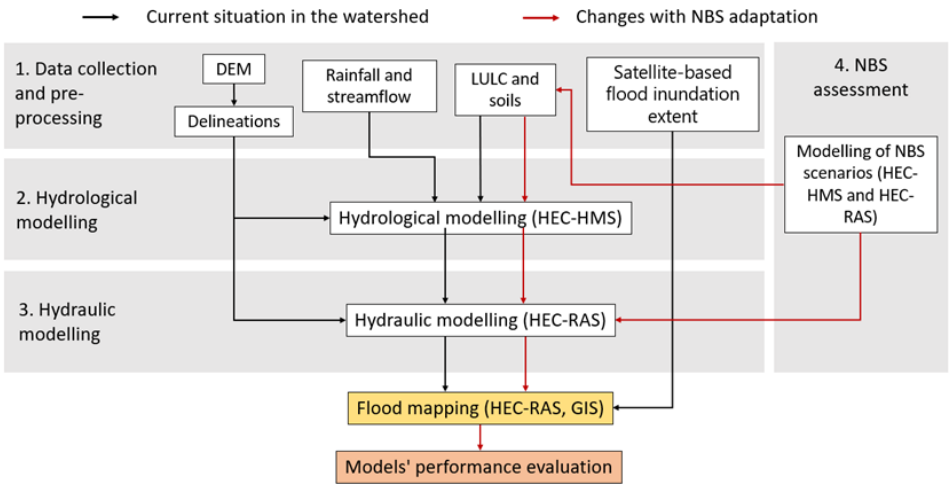

Figure 3. The workflow of an integrated hydrologic–hydraulic model developed in this research.

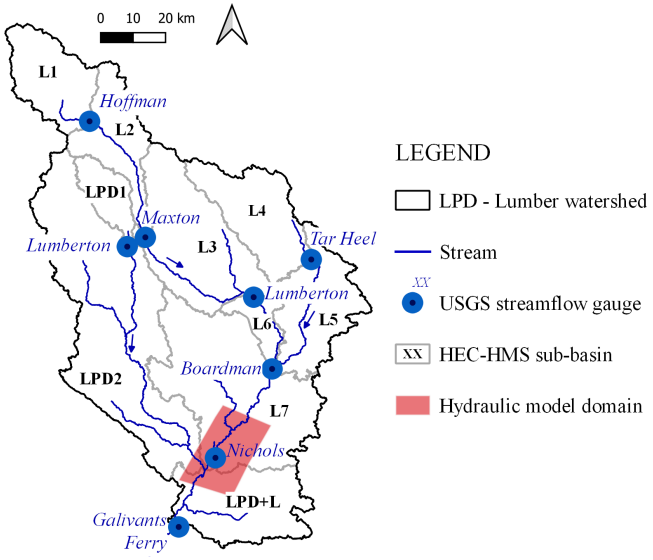

Figure 4. Sub-basins and hydraulic model domain.

A weighted average CN number is calculated for each sub-basin based on the hydrologic group and LU types, according to the values in Table 3. As described in the "Study case and data collection" section, the area is principally covered by wetlands, croplands, and forests, and the typical hydrological soil groups (HSGs) are A/D, B/D, and C/D.

The CUH method was adopted to model direct runoff. Clark's model derives a catchment UH by explicitly representing two critical processes in the transformation of excess precipitation to runoff (US Army Corps of Engineers, 2021):

- translation or movement of the excess from its origin throughout the drainage to the watershed outlet and
- attenuation or reduction in the magnitude of the discharge as the excess is stored throughout the watershed.

Table 3. CNs adopted for each LULC and HSG with AMC II (Emergency Management NC, 2018; US Army Corps of Engineers, 2021).

LU type	Hydrologic group			
	A	B	C	D
Open water	100	100	100	100
Developed, open space	49	69	79	84
Developed, low intensity	57	72	81	86
Developed, medium intensity	61	75	83	87
Developed, high intensity	77	85	90	92
Barren land	77	86	91	94
Deciduous forest	36	60	73	79
Evergreen forest	36	60	73	79
Mixed forest	36	60	73	79
Shrub/scrub	35	56	70	77
Herbaceous	30	58	71	78
Hay/pasture	39	61	74	80
Cultivated crops	64	74	81	84
Woody wetlands	88	89	90	91
Emergent Herbaceous Wetlands	88	89	90	91

It seems both mechanisms actively control rainfall–runoff processes in our study area. The model requires two input parameters: the time of concentration (T_c) and the storage coefficient I. T_c was initially estimated using the SCS lag equation developed by the SCS (1972). The SCS recommends that the lag equation (Eq. 1) be used on basins that may be considered homogeneous in nature and that are less than 800 hectares in size. Due to these restrictions, the method may be limited for application on most basins; however, it has widely been used and accepted around the world for catchments of varying sizes (Soulis, 2021; Mishra and Singh, 2003; Knebl et al., 2005), and it has been used in the study area for a similar application (Emergency Management NC, 2018). We

used this approach for an initial estimation of the values. The equation uses the path length of the stream in feet (L), the potential maximum retention in inches (S), and the average watershed land slope in percent (Y) to estimate the lag time in hours (T_{lag}) (US Army Corps of Engineers, 2021):

$$T_{\text{lag}} = \frac{L^{0.8}(S+1)^{0.7}}{1900 \cdot Y^{0.5}}. \quad (1)$$

Then, the time of concentration can be derived from $T_{\text{lag}} = 0.6T_c$.

The initial estimation for the storage coefficient I was estimated using the following relationship (US Army Corps of Engineers, 2021):

$$\frac{R}{T_c + R} = 0.6. \quad (2)$$

The exponential recession method was used to represent watershed baseflow. It requires the initial flow (Q_0), the recession ratio (k), and the ratio to peak as input parameters (US Army Corps of Engineers, 2021).

For channel routing simulation, the Muskingum method was selected. This method uses a simple finite-difference discretization of the continuity equation to route an inflow hydrograph. The method aims to capture during the simulation the observed increase and decrease in channel storage during the passing of a flood wave. The required parameters for the method are the travel time (T) of the flood wave through any reach and a dimensionless weight X that can range from 0 to 0.5.

Two hurricane types with similar durations and rainfall intensities were considered in this study. Although, the angles of landfall and storm tracks were different for each of them. In this way, the different spatial and temporal variabilities of hurricanes and how they affect the watershed's response to flooding could be analyzed. The selected hurricanes were Matthew and Florence. Hurricane Matthew had a coast-parallel storm track with higher cumulative precipitation volumes in the south of the watershed. In contrast, Hurricane Florence had a meandering storm track with greater precipitation rates on the east side of the watershed, resulting in extremely large flows in all the tributaries. Hurricane-force winds extended outward up to 110 km from the center during Hurricane Florence (National Hurricane Center, 2018) and up to 75 km during Hurricane Matthew (NASA, 2016). Williams et al. (2020) examined the rainfall volumes during the month of occurrence of the hurricanes and in the previous month. They discovered that rainfall in the watershed 1 month before Hurricane Matthew was nearly equal to the month of the hurricane, placing wet soil moisture conditions for the hurricane month. On the contrary, before Hurricane Florence, the watershed received little rainfall, leading to drier soils during the hurricane event.

The two simulated events are separately calibrated. The calibration process attempts to reproduce the peak discharges and total flood volumes at all the flood gauges in the watershed. Calibration was achieved by adjusting the CNs, time of concentration, storage coefficient, baseflow, and channel routing parameters in each sub-basin. The calibration was performed with a time interval of 15 min, and the calibration periods were

- 6–31 October 2016 and
- 14 September–5 October 2018.

3.2 Hydraulic modeling

The HEC-RAS version 6.2 was used to develop the hydraulic model. A 1D simulation was performed, which executes surface profile calculations in a gradually varied flow. The program solves water surface profiles from one cross section to the other by solving the energy equation.

The hydraulic model domain was restricted to a small area in the proximity of Nichols; 20 km of the Lumber River was modeled upstream of the town and 20 km more downstream to include the confluence with the LPD River (see Fig. 4).

To generate the HEC-RAS geometric input data, the triangular irregular network (TIN) was obtained from the 10×10 m DEM. The main channel, riverbanks, and flow paths were created using georeferenced information from the National Hydrography Service (NHS) and manually adjusted with the aerial image to follow the river path more precisely. The channel width was visually compared with Google Satellite images. Although there are no measured geometry data of the river and floodplain cross sections, $3\,\text{m} \times 3\,\text{m}$ DEM data are available in some portions of the watershed, and they were used for correcting the main channel sections. The river's cross sections were generated every 2000 m, and, at Nichols, the resolution was increased by placing the cross sections every 1000 m. The upstream boundary conditions for the model are the discharges simulated with the HEC-HMS in the Lumber River and the LPD River, while the normal depth was used as the downstream boundary condition.

Manning's roughness coefficient was automatically assigned in the cross sections from the land use map in HEC-RAS. The software calculates a weighted average of n in each cross section, taking into consideration the different LULC types. Each LULC type was designated a manning roughness coefficient following Table 4 (Emergency Management NC, 2018; US Army Corps of Engineers, 2021).

3.3 Performance metrics

The validation of the model was assessed by comparing the simulated and observed flood inundation areas from satellite images for hurricanes Florence and Matthew. The simulated flood inundation maps of both hurricanes were transferred from HEC–RAS to a GIS environment as raster files to process and compare with the observed data. Flood mapping performance is evaluated by using categorical verification

Table 4. Manning's roughness coefficients according to LULC type.

LULC	Normal n value[1]	Allowable range of values[2]
Developed	0.12	0.03–0.2
Evergreen forest	0.15	0.1–0.16
Grassland/herbaceous	0.035	0.025–0.05
Cultivated crops	0.05	0.025–0.05
Woody wetlands	0.07	0.045–0.15
Emergent herbaceous wetlands	0.045	0.05–0.85
Main channel	0.035	

[1] US Army Corps of Engineers (2016). [2] NRCS Kansas (2016).

statistics, which are usually implemented for estimating the accuracy of flood forecasts (Bhatt et al., 2017; Bhattacharya et al., 2019). The categorical verification statistics measure the correspondence between estimated and observed inundation patterns. In this study, the probability of detection (POD; Eq. 3), false alarm ratio (FAR; Eq. 4), and critical success index (CSI; Eq. 5) were used. The POD indicates what fraction of the observed inundation was correctly simulated. The FAR indicates what fraction of the simulated inundation did not occur. The CSI indicates how well the simulated and observed inundation fit.

$$\mathrm{POD} = \frac{\text{hits}}{\text{hits} + \text{misses}} \tag{3}$$

$$\mathrm{FAR} = \frac{\text{false alarms}}{\text{hits} + \text{false alarms}} \tag{4}$$

$$\mathrm{CSI} = \frac{\text{hits}}{\text{hits} + \text{misses} + \text{false alarms}} \tag{5}$$

The observed and simulated inundation polygons were intersected to find areas of hits, misses, and false alarms. These are defined in the following way:

- Hits are when a grid cell in the satellite image shows wet and in the simulated inundation map shows wet.
- False alarms are when a grid cell in the satellite image shows dry and in the simulated inundation map shows wet.
- Misses are when a grid cell in the satellite image shows wet and in the simulated inundation map shows dry.

In addition, this study used a variety of performance metrics for model benchmarking, including the Nash–Sutcliffe efficiency (NSE; Eq. 6; Nash and Sutcliffe, 1970), root mean square error (RMSE; Eq. 7), correlation coefficient (R^2; Eq. 8), and the flood peak relative error (PE; Eq. 9):

$$\mathrm{NSE} = 1 - \frac{\sum_{i-1}^{n} (P_i - O_i)^2}{\left(O_i - \overline{O}\right)^2}, \tag{6}$$

$$\mathrm{RMSE} = \sqrt{\frac{\sum_{i=1}^{n} (O_i - P_i)^2}{n}}, \tag{7}$$

$$R^2 = \frac{\sum \left(O_i - \overline{O}\right)\left(P_i - \overline{P}\right)}{\sqrt{\sum \left(O_i - \overline{O}\right)^2 + \sum \left(P_i - \overline{P}\right)^2}}, \tag{8}$$

$$\mathrm{PE} = \frac{O_{\mathrm{peak}} - P_{\mathrm{peak}}}{O_{\mathrm{peak}}}, \tag{9}$$

where P and O represent simulated and observed stream discharges, respectively.

3.4 NBS assessment

The methodology used to assess the implementation of NBSs as flood mitigation measures in the watershed consists of the following steps:

1. Selection of NBS measures
2. Site suitability analysis of selected NBS measures
3. Development of NBS scenarios
4. Modeling of scenarios in an integrated hydrologic and hydraulic model

3.4.1 Selection of NBS measures

The chosen NBSs should be appropriate for implementation in the watershed and feasible to include in the hydrologic and hydraulic models. They should also be feasible to be applied in large and undeveloped areas. Three NBS measures were selected for the study area which have proven to be correctly implemented in HEC-HMS and HEC-RAS models in various cases (Brink et al., 2016; Thomas and Nisbet, 2007). They are offline flood storage ponds, riparian reforestation, and afforestation in croplands.

Flood storage ponds are used both to attenuate the incoming flood peak and to delay the timing of the flood so that the volume is discharged over a longer period. Offline storage is usually located within the floodplain of large rivers with wide floodplains. In these structures, the water is diverted from the river channel, stored, and slowly released back into the river (Ecologic Institute, 2019). HEC-RAS v6.2 includes a module intended particularly for incorporating storage areas into the model.

According to the examination of LULC information, there has been a significant decline in forested regions and woody wetlands during the past two decades. Afforestation can help

not only reduce runoff volume by enhancing water absorption and interception but also reduce water velocities. The afforestation measures can be very easily implemented in the hydrologic and hydraulic models compared to other types of natural infrastructure.

3.4.2 Site suitability analysis

A site suitability analysis was conducted for defining the areas where selected NBSs can be implemented. The domain for allocation of NBSs was considered upstream of Nichols, in the Lumber River watershed between Nichols and Lumberton (Lumber sub-basins 6 and 7) and Big Swamp Creek (Lumber sub-basins 4 and 5).

According to Mubeen et al. (2021), the most common criteria to determine NBS site suitability are slope, soil type-/class, imperviousness, distance from the stream, land use type/zone, urban land use, and road buffer. Based on the results of Mubeen et al. (2021), the following parameters were chosen to determine the suitable areas for the development of storage ponds and riparian reforestation:

- slope $< 5\,\%$,
- pervious areas,
- distance from main river < 1000 m or inside floodplain,
- distance from roads > 50 m,
- LULC type outside of forested areas or woody wetlands.

The analysis of site suitability was performed in a GIS environment. The slope was derived from the DEM, pervious areas were derived from imperviousness maps, forested areas and woody wetlands from LULC maps, and stream and road distances from buffers of the georeferenced data. From each criterion, raster maps were developed and then transformed into Boolean maps showing areas where each condition is met. The combination of these maps produces a general suitability map where ponds or riparian vegetation can be allocated. The general suitability map was combined with measuring specific criteria for riparian reforestation, which allowed for the separation of those areas from the storage pond areas (Fig. 5). This criterion is to restore riparian forests to the situation of the year 2001. A separate map for afforestation in croplands was developed; in this case, the suitable areas are all the croplands in the considered sub-basins (Fig. 6).

3.4.3 Development of NBS scenarios

Four NBS scenarios were developed in this research.

- *Scenario 1, offline flood storage pond.* This scenario consists of one offline flood storage pond located on the right margin of the Lumber River floodplain near Nichols. Conceptually, the storage pond would involve constructing a 1 m high berm around the perimeter of the pond area, with inlet and outlet structures from and towards the Lumber River.

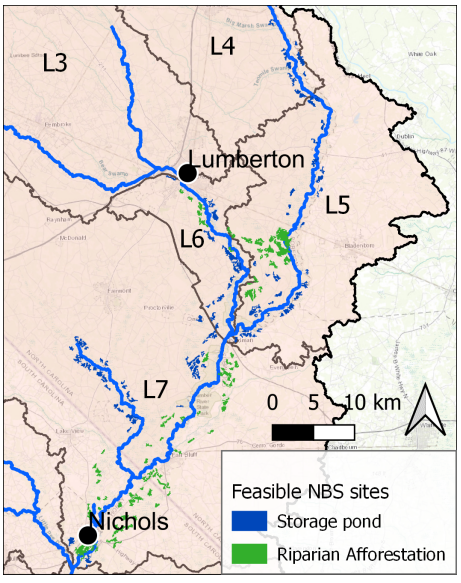

Figure 5. Feasible sites for storage ponds and riparian reforestation (original LULC layer extracted from MRLC consortium).

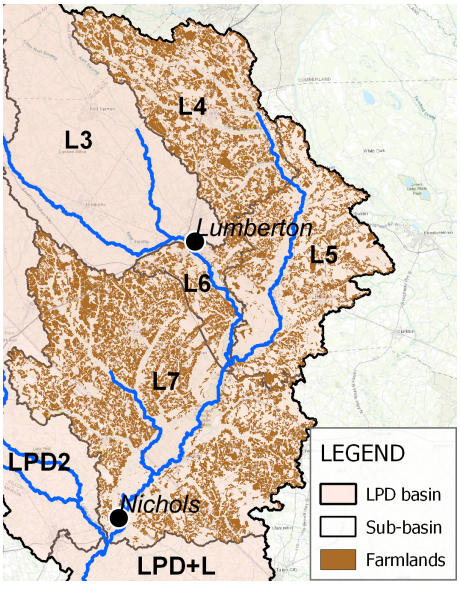

Figure 6. Feasible sites for afforestation in croplands (original LULC layer extracted from MRLC consortium).

- *Scenario 2, riparian reforestation.* For the riparian reforestation scenario, forested areas were restored to their previous state in 2001 inside the floodplain areas. Overall, 23 km^2 of the watershed were converted to forests in this scenario, influencing the CN of the watershed.

- *Scenario 3, afforestation in croplands*. The conversion of cropland areas to forests also influences the CN of the watershed due to changes in LULC. Three sub-scenarios were developed according to the percentage of cropland area converted to forest:
  - Scenario 3a: changing 10 % of the cropland area to forest, 96 km^2 afforested.
  - Scenario 3b: changing 20 % of the cropland area to forest, 144 km^2 afforested.
  - Scenario 3c: changing 50 % of the cropland area to forest, 192 km^2 afforested.
- *Scenario 4, combination of scenarios 1, 2, and 3*. This scenario is the combination of all three proposed NBSs together.

3.4.4 Scenario modeling

The NBS scenarios were tested on the Hurricane Matthew event, given its elevated performance in inundation modeling for the base scenario compared to Hurricane Florence. The same process for flood mapping was followed as in the base scenario but with new adjustments to the hydrologic and hydraulic models. The afforestation scenarios were evaluated with the new CN in HEC-HMS, the new results were used as inputs for the hydraulic model, and new flood maps were obtained. Regarding the flood pond, the scenario was directly evaluated in HEC-RAS. The storage areas, incorporated in the software, create lake-like regions that water can be diverted into or from (US Army Corps of Engineers, 2016). The reduction in discharge and flood inundation over Nichols were compared with the base scenario to assess the NBS performance.

4 Results

This research contributes to the literature on the modeling of NBS measures at a catchment level, which proved useful to mitigate, to a certain extent, hurricane-driven flooding events. We determined a methodology for selecting, modeling, and evaluating the performance of NBSs within a catchment, which can also be extended to other case studies. Another expectation of this research is that it can help decision-makers to define proper flood risk management strategies. The modeling techniques and methodology proposed for the NBS implementation can be of interest to flood/stormwater modelers, and the results can broadly be integrated with the government effort for flood mitigation plans. While severe damages were reported in many parts of the LPD watershed, a lack of proper studies and research in the area hinders the process of implementing flood reduction measures. This research contributes to identifying at-risk areas that can potentially be stabilized by the NBS measures.

4.1 Hydrological modeling

The LPD–Lumber watershed was modeled in HEC-HMS and divided into 10 sub-basins. Each sub-basin was considered to be a lumped model where the runoff at the outlet was estimated from the input rainfall and calibrated with a streamflow gauge.

For the SCS CN method, a composite CN value was calculated for each sub-basin, weighting the CNs by the area of different LULC classes in the sub-basin. The LULC classes were assigned a CN based on the tables developed by the SCS and from recommendations of other case studies in the US (US Army Corps of Engineers, 2021). The initial estimations of composite CNs in the sub-basins varied between 57.7 to 80.4.

For the runoff transformation model, the CUH was adopted. The initial estimations for the time of concentration ranged from 26 to 64 h, while the storage coefficient varied between 36 to 96 h through the sub-basins.

For the estimation of the baseflow, the exponential recession method was used. The initial flow is an initial condition estimated as the average flow on the day before the start of the storm. The recession constant k and the ratio to peak were initially estimated at 0.95 and 0.25, respectively, values recommended by the HEC-HMS technical reference manual (US Army Corps of Engineers, 2021). These values were later adjusted during the calibration process.

For the channel routing, the Muskingum method was selected. The travel time of the flood wave through the reach K was estimated as the interval between similar points on the inflow and outflow hydrographs of the sub-basin. The dimensionless weight X was initially estimated at 0.5 as recommended by the HEC-HMS technical reference manual (US Army Corps of Engineers, 2021), and its value was later adjusted in the calibration.

The calibration was performed using an automatic process based on the Simplex search algorithm, minimizing the peak weighted RMSE at all streamflow stations. The calibration process consisted of, firstly, defining model parameter constraints and, secondly, automatically calibrating each sub-basin progressively from upstream to downstream. The parameter constraints were selected from other case studies, suggestions, and information about the watershed. It is desired that the estimated parameters do not vary far from the estimated values (only around 20 %), but individual exceptions were considered to accommodate the watershed's special characteristics. As indicated before, the watershed has a considerable effect on ponding and water detention due to its topography, vegetation, and soil types. This significantly influences the water volumes that reach the stream and its travel times. To accommodate this effect, large values were permitted for the storage coefficient and time of concentration, while low values were allowed for CN. The ranges for the recession constant, ratio to peak, and attenuation factor were obtained from recommendations in the HEC-HMS manual

Table 5. Accuracy ranges of hydrological simulations at all flood gauging stations.

Variable	Hurricane Matthew	Hurricane Florence
RMSE/avg	11 %–38 %	13 %–64 %
NSE	0.89–0.99	0.89–0.99
R^2	0.94–0.99	0.90–0.98
Flood peak error	2.2 %–7.4 %	7.2 %–11.3 %

(US Army Corps of Engineers, 2021). The calibration procedure was performed by automatically calibrating the parameters of each sub-basin. If the sub-basin had a flood gauge at the outlet, the parameters were calibrated individually. If not, more than one sub-basin was calibrated simultaneously. Calibration was conducted from upstream to downstream in a stepwise manner.

Figures 7, 8, and 9 show the simulated hydrographs for hurricanes Matthew and Florence at the eight flood gauging stations. In general, the trend of the observed hydrographs was calibrated well in both hurricane models. The obtained calibration accuracies are good according to the performance metric results shown in Table 5.

The calibrated parameters show specific trends that permit a comparison of both hurricanes' behaviors. Matthew's model calibration required higher values of CN than Florence's model, possibly indicating wetter antecedent moisture conditions (AMCs) during the former event. This observation matches other studies regarding these storms in the Lumber River (Emergency Management NC, 2018; Doll et al., 2020) and agrees with the findings of Williams et al. (2020) highlighting the large rainfall volumes of the month before Hurricane Matthew. Additionally, it was observed that most of the calibrated CN values are in the estimated range between dry and normal AMCs in both hurricane simulations. This effect can be attributed to dry AMCs in the watershed soils; however, this contradicts the previous findings of a wet month prior to Hurricane Matthew. Another explanation can be attributed to the water detention and ponding effects, which are expected to decrease the total runoff volumes of the watershed. Also, water detention and ponding effects can influence the calibrated storage coefficients and times of concentration, which resulted in generally higher calibrated storage coefficients and times of concentration than those initially estimated.

The hydrograph at the Lumberton flood gauge showed a bimodal behavior with two evident flood peaks, one occurring on the day of the peak rainfall and the second occurring between 3 to 4 d later (see Fig. 7). It was assumed that the first peak corresponds to the response of the sub-basin to flooding, while the second peak was generated by the delayed flow originating from upstream portions. The travel time values in the upper watershed were much larger than expected, with travel times from Hoffman to Maxton and from Maxton to Lumberton gauges ranging between 2 to 3 d. The peaks at Hoffman, Maxton, and Lumberton were around 40 % lower during Hurricane Matthew compared to those during Hurricane Florence. This observation matches the results from the rainfall interpolations that show less concentration of rainfall volumes in the north of the watershed during Hurricane Matthew.

During Hurricane Florence, the first and the highest peak at Lumberton was generated by the Lumber 3 sub-basin runoff (see Fig. 4). This highest peak, together with the input from the Big Swamp Creek (Tar Heel hydrograph), created the flood peak observed at the Boardman gauge (Fig. 8). The second and the smaller peak observed at the Lumberton gauge does not contribute to the main flooding peak at any of the downstream gauges. However, it caused a slower recession of the hydrograph in the downstream portion of the watershed (Fig. 9), thereby increasing the flooding lead time in that portion.

This simulation shows that the simultaneity of peak flow occurrence from the LPD and Lumber rivers during Hurricane Florence is one of the reasons for the high flood peak rate at the river's intersection as reported elsewhere (Muller, 2020). During Hurricane Matthew, the LPD River peak arrived 2.5 d earlier than the peak from the Lumber River, while for Hurricane Florence they occurred within a period of just a few hours. The peak flows and time to peak are presented in Table 6.

4.2 Hydraulic modeling

The hydraulic model requires separate roughness coefficients for floodplains and the main channel. In the floodplains, Manning's roughness coefficient was automatically assigned in the cross sections using the LULC map following Table 7. For the main channel, a Manning coefficient of 0.35 was selected.

The calibration process attempts to reproduce the observed peak water level at Nichols for Hurricane Florence. This is managed by manually adjusting Manning's roughness coefficient of the woody wetlands, which is the land use type with the largest area in the model domain and for which the results show the most significant sensitivity. The water elevation observed at the Nichols gauge during Hurricane Florence was 17.0 m above NAVD 88. The calibrated Manning's roughness coefficient of woody wetlands resulted in a value of 0.09, which is within the allowable range of values according to Table 7.

The flood inundation maps of both hurricanes are shown in Fig. 10. Water depths reached up to 4.5 m and velocities up to 1.7 m s^{-1} during Hurricane Florence and up to 4.4 m and 1.6 m s^{-1} during Hurricane Matthew. During both events, Nichols was severely inundated, causing severe damage to properties, businesses, and residential homes.

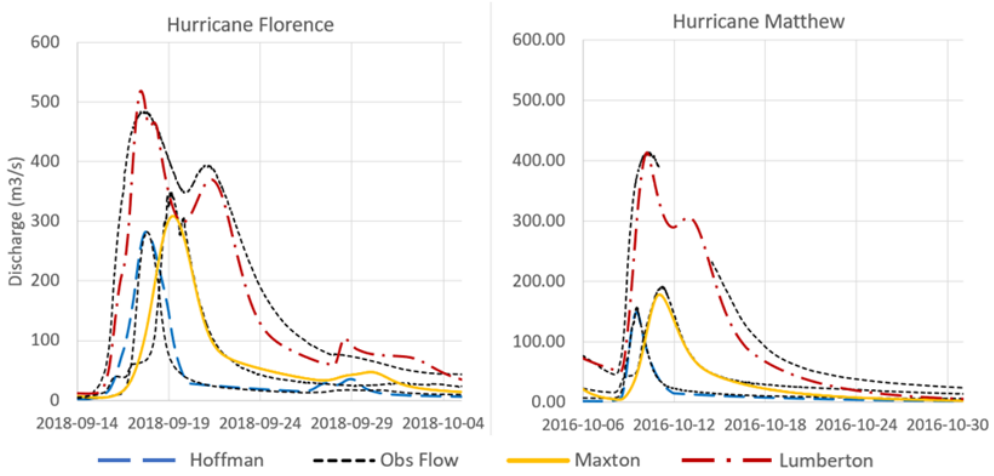

Figure 7. Observed and simulated flood hydrographs at the Hoffman, Maxton, and Lumberton stream gauges.

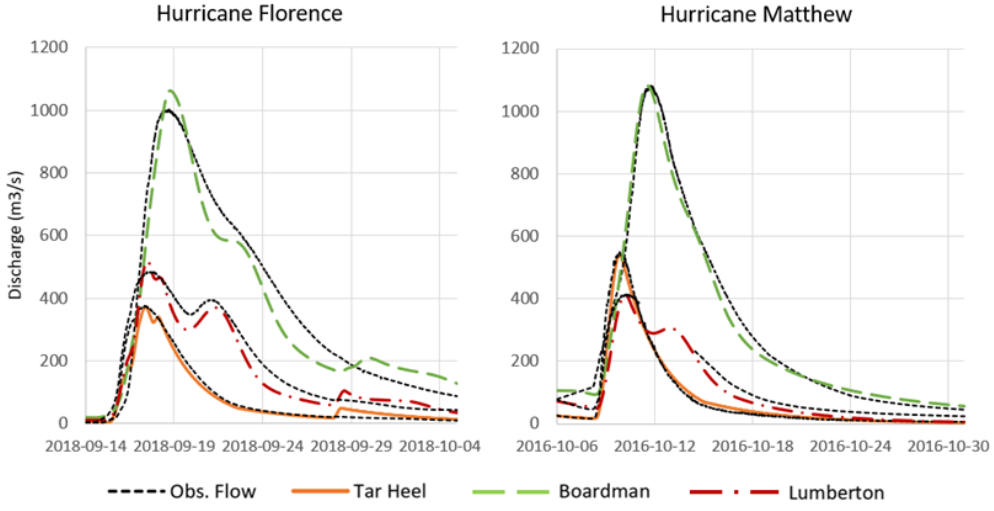

Figure 8. Observed and simulated flood hydrographs at the Tar Heel, Lumberton, and Boardman stream gauges.

4.3 Validation of flood inundation

Figure 11 presents the calculated false, correct, and missed alarms that are compared with the observed inundations. These areas are used to calculate the categorical verification statistics which resulted in, for Hurricane Matthew, POD = 79 %, FAR = 20 %, and CSI = 67 %, while for Florence they were POD = 83 %, FAR = 51 %, and CSI = 45 %. The higher the values of CSI and POD are, the more accurate the model is, and the opposite is true for FAR. It can be inferred that the simulated inundation extents showed a good match with the observed satellite images for Hurricane Matthew and less good for Florence. The PODs are high for both events, while CSI is only high for Matthew. Furthermore, the FAR value is low for Hurricane Matthew but for Florence is more than 50 %.

There are several reasons why Hurricane Florence's inundation mapping was less accurate. It is possible that the inaccuracy was produced by errors in the observed satellite image, caused by cloud obstructions during the hurricane event. After analyzing the satellite images provided by the Flood Observatory for the Hurricane Florence event, discordances were found with other observed and measured data. A comparison of both hurricanes' flood inundation maps was conducted to understand the similarities and differences (see Fig. 12). While comparing the satellite observations of hurricanes Florence and Matthew, it was found that the flooding extent for Matthew's event around Nichols is much bigger than the one during Florence and that the satellite-observed flood extent of Hurricane Florence does not cover Nichols, contradicting other more reliable sources of information.

It is also possible that the inaccuracies are caused by the model setup, which could not capture all features of the terrain, such as the existence of structures built along the river, after Hurricane Matthew.

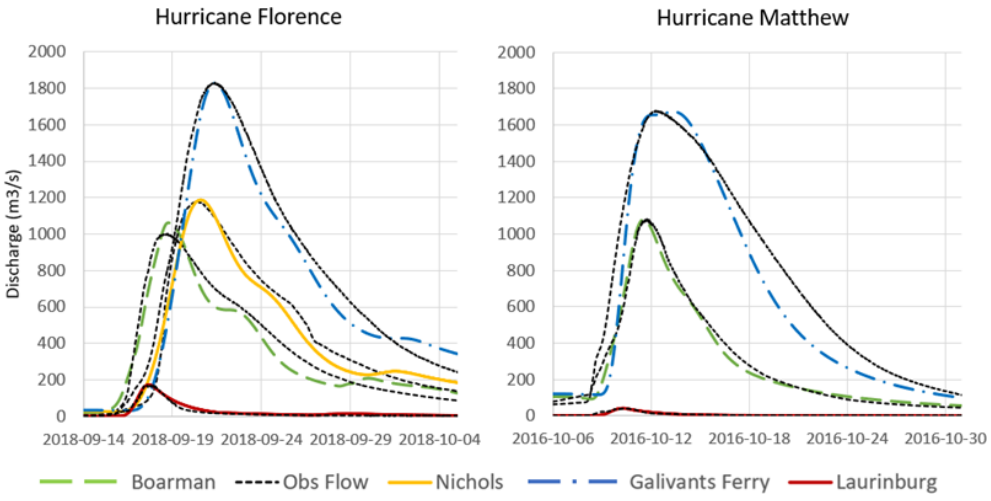

Figure 9. Observed and simulated flood hydrographs at Laurinburg, Boardman, Nichols, and Galivants Ferry.

Table 6. Simulated flood peaks at the LPD and Lumber intersection.

Simulation	River	Peak flow ($m^3\ s^{-1}$)	Peak time
Hurricane Matthew	Lumber	1248	12 October 2016 23:30 LT (GMT−4)
	LPD	566	10 October 2016 14:45 LT
	Lumber + LPD	1678	12 October 2016 10:45 LT
Hurricane Florence	Lumber	1187	20 September 2018 15:15 LT
	LPD	689	20 September 2018 02:30 LT
	Lumber + LPD	1859	20 September 2018 11:00 LT

Table 7. Manning's roughness coefficients by LULC type.

LULC	Normal n value[1]	Allowable range of values[2]
Developed	0.12	0.03–0.2
Evergreen forest	0.15	0.1–0.16
Grassland/herbaceous	0.035	0.025–0.05
Cultivated crops	0.05	0.025–0.05
Woody wetlands	0.07	0.045–0.15
Emergent herbaceous wetlands	0.045	0.05–0.85
Main channel	0.035	

[1] US Army Corps of Engineers (2016). [2] NRCS Kansas (2016).

4.4 NBS performance

The performance of NBS scenarios is evaluated based on their ability to reduce the inundation area at Nichols for Hurricane Matthew. The total built-in area of the town was estimated at 122 ha. For the base scenario, the model simulation shows that 56 % of the town's area was inundated during Hurricane Matthew. With the NBS scenarios, the inundated area was reduced to a range of 55 % to 38 %. The results for NBS scenarios and the maximum water depth at the USGS gauge are shown in Table 8. The effects of flood storage ponds as well as riparian reforestation are almost neglectable, with an insignificant reduction in flood peak rate and inundation area.

When the afforestation was implemented in a large domain in the model, such as those of Scenario 3, the effects start to be visible. These measures showed reductions ranging between 8 % and 18 % in the inundated urban area. However, still, 38 % of the town is at risk of flooding even when afforestation was largely implemented in the model. The reason for this could be that the whole area in the downstream catchments is quite flat, not allowing for great improvements unless great amounts of water are captured upstream. Furthermore, an optimization of the location of these forested areas could improve the results. NBSs work better when applied upstream in the catchment. Nevertheless, this study focuses on the effects in downstream areas because Nichols is located there.

Scenario 4 gives comparable results to those in Scenario 3, given that the first two scenarios have an extraordinarily insignificant effect on the results.

Table 8. Flood reduction performance of the scenarios.

Scenario	Area inundated in Nichols (Ha)	% of Nichols area	Flood peak depth at Nichols gauge (m)
Base scenario	68.4	56 %	3.15
Scenario 1: pond	67.6	55 %	3.14
Scenario 2: riparian reforestation	66.2	54 %	3.12
Scenario 3a: afforestation, 10 %	59.1	48 %	2.96
Scenario 3b: afforestation, 20 %	56.3	46 %	2.94
Scenario 3c: afforestation, 50 %	46.7	38 %	2.84
Scenario 4c: Sc. 1 + Sc. 2 + Sc. 3	44.3	36 %	2.82

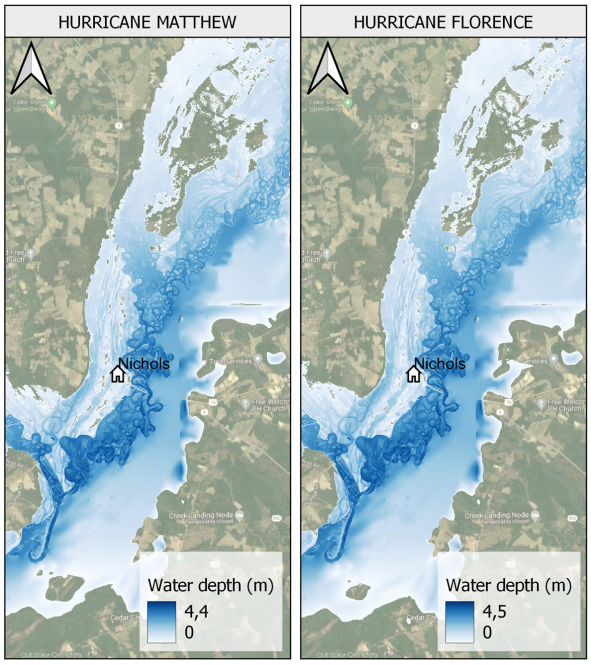

Figure 10. Simulated flood depth during hurricanes Matthew and Florence in Nichols (© Google Maps 2022).

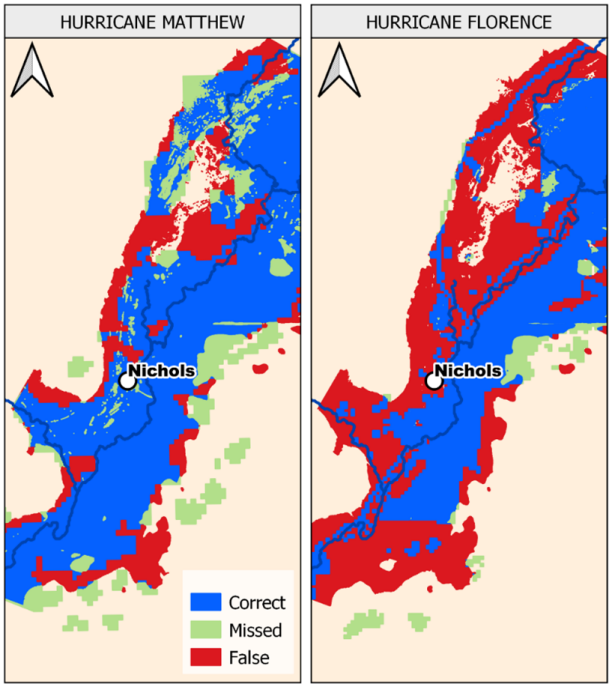

Figure 11. Correct, missed, and false alarm areas in Nichols.

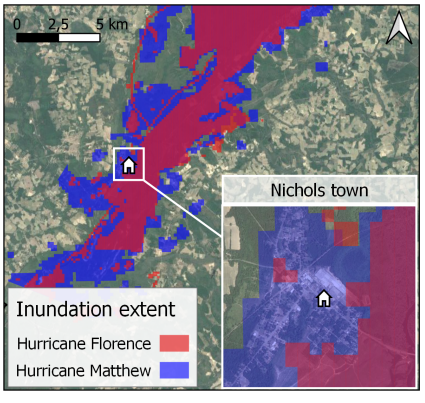

Figure 12. Observed flood extent for hurricanes Matthew and Florence (layers from Dartmouth Flood Observatory, 2016, 2018).

With regard to the reduction in flood peak depths, the NBS measure of reforestation on floodplains (Scenario 2) showed an insignificant impact. However, the alternatives in Scenario 3 performed higher peak reductions, ranging between 2.2 % and 13 %.

5 Conclusions and future works

This study developed an integrated hydrologic–hydraulic modeling system for hurricane-driven flood simulation and discussed how NBS measures can be implemented in the proposed modeling system to mitigate flood peak rates and inundation areas. The present study can serve as an example of application and methodology to areas with similar physical characteristics in the world. The catchment character-

istics that are important when replicating the methodology are large storage and long detention times, which are also affected by hurricanes or similar storms. Data availability needs to be similarly rich. The extension of these models to less intense storms or areas with steeper slopes needs to be further investigated. Furthermore, this research adds to the scientific literature on modeling NBS measures at a catchment level, which proved useful to mitigate hurricane-driven flooding events.

Despite the challenges associated with flood modeling in the LPD–Lumber River watershed, the model performed well. However, different complexities made modeling a challenging task. The watershed is a challenging hydrologic system due to its physical characteristics, which make it prone to surface ponding conditions with long residence times. The effects of complex floodplain response, dense vegetation, gentle slope that increases flood ponding/residence time, uncertainty in rainfall and flood variability/distribution as well as reservoir operation can significantly impact the modeling outcomes. Although, the calibration of hurricanes Florence and Matthew in separate models was performed with good accuracy.

It was discovered that calibrated CN values for both events were lower than those predicted in most sub-basins for normal AMCs. A severe dry AMC in the watershed could be the cause of this or, perhaps (since no evidence suggests dry AMC), the Pee Dee area's typical attenuation and detention effects. The flow attenuation effects may also explain the long response times observed in most of the sub-basins. The time between peak occurrence at consecutive flood stations varies across rainfall events, which may be attributed to differences in reservoir operations and initial water content in detention areas.

Water attenuation and detention effects in the upper sub-basins of the Lumber River have a direct impact on increasing the recession periods of the hydrographs in the lower sub-basins. The delayed response from the upper Lumber River created a double peak effect at the Lumberton flood gauge. In both hurricane events, the first and the highest peak rates were generated at the Boardman outlet, which largely raised the total flood peak downstream, while the second peak contributed to generating a smooth and slow decrease at the falling limb of the hydrograph, lengthening the time the river takes to get back to its normal flow.

The spatial and temporal patterns of rainfall for both hurricane events play a key role in the generation of flood hydrographs. Higher rainfall volumes concentrated in the south of the watershed during Hurricane Matthew implied that the flood peak at Nichols was mostly due to the Lumber River and less the LPD. On the contrary, during Hurricane Florence, the whole watershed received higher rainfall amounts, principally in the east. This generated a higher flood peak at the intersection of the LPD and Lumber rivers, caused by simultaneous peaks originating from both rivers.

The simultaneous occurrence of flood peaks from the LPD and Lumber rivers caused the inundation extension to be larger during Hurricane Florence than during Hurricane Matthew. According to the simulated events, Hurricane Matthew inundated 58 % of Nichols' residential area, whereas Hurricane Florence inundated 91 %. In the model domain, simulated water depths and velocities reached 4.5 m and $1.7\,\mathrm{m\,s^{-1}}$ for Hurricane Florence and 4.4 m and $1.6\,\mathrm{m\,s^{-1}}$ for Hurricane Matthew.

The performance of flood inundation mapping revealed high accuracy for Hurricane Matthew, while showing less accurate results for Hurricane Florence. The deficient performance of Hurricane Florence is attributed to the observed data rather than simulation errors. The flood extent observations during Florence were not validated against other satellite images due to cloud coverage, as the images mismatched the archived photos of Florence-driven inundation and neighbor testimony.

The NBS scenario simulation indicated neglectable flood reduction outcomes for the flood storage pond and riparian reforestation, while afforestation in the cropland scenario had a more visible effect. The storage pond worked correctly throughout the simulation; however, the flow that must be decreased to minimize inundation in Nichols is overwhelmingly high to manage using a single flood storage pond. The NBS site suitability analysis revealed more potential locations outside of Nichols where ponds can be designed and implemented, allowing for a higher number of storages to be considered.

The afforestation in cropland scenarios revealed the best flood reduction results of any intervention tested. This is because it operates at a much higher scale, which is required in this situation to observe an effect on flood reduction. Evidently, the more cropland area was converted to forests, the more reduction in flood peak rate and volume was observed. Although, these findings should be accompanied by an evaluation of the cropland surface area that can be realistically transformed into forests.

The selected loss method (SCS CN) in the HEC-HMS model did not allow for the consideration of the sub-basins' initial conditions in terms of soil moisture (unless CNs are adjusted for each event) and water table elevation. In addition, the HEC-HMS model is unable to account for reservoirs or other detention areas in a direct manner, and the initial water contents of these areas, which could potentially influence simulation results, are uncertain. To account for these uncertainties, water detention in the sub-basins is manually formulated into an equation in the calibrated parameters of CN, time of concentration, and storage coefficients. In this region, dense vegetation and extensive forested/non-forested wetlands may severely impact runoff generation. These complexities along with poor natural drainage created an excessive soil water condition that is difficult for the model to understand and capture their dynamics and interaction. Dense vegetation and forested/non-forested wetlands affect the vari-

able source area involved in the generation of saturation overland flow, and this mechanism can cause the rainfall–runoff module to behave chaotically during flood simulation.

Another difficulty that concerned us was the lack of sub-daily rainfall data at some sub-basins, which made the modeling and understanding of the runoff generation mechanism difficult. In this case, it is important to model the watershed for other significant flooding events when the rainfall distribution over the watershed is different from hurricanes Matthew and Florence. In addition, several modeling improvements could be explored in the future. For example, a continuous simulation with a soil-moisture-accounting model as a loss method could be tested to help improve modeling results.

The large quantity of storage facilities within the catchment likely has a substantial impact on the modeling process. We recognize a limitation in our study regarding the functioning of these reservoirs. Due to the sensitive nature of operating such structures during hazardous conditions, information regarding their operation is not accessible to the public.

We acknowledge that both hydrologic and hydraulic simulations can be made more efficient by coupling these models with Bayesian uncertainty inference such as Bayesian model averaging (BMA; Samadi et al., 2020) and/or Markov chain Monte Carlo (MCMC) optimization methods (Duane et al., 1987). The analyses presented herein are intended to provide a basis for NBS implementation and assessment in both hydrologic and hydraulic settings. However, subsequent in-depth studies are needed to examine the impacts of individual and combined NBS measures on flood peak and volume reduction. Additionally, checking the emergent behavior of the hydrograph (in more detail) over time using carefully designed in-filed NBS implementation is useful to expose key runoff generation mechanisms in at-risk watersheds. Acknowledging a growing enthusiasm for NBS modeling studies in the hydrology community, we expect progress on multiple fronts: a better module to design NBS structures in the model, better accuracy metrics for quantifying NBS performance, and better error estimation of NBS implementation. As always, we invite dialogue with hydrology communities interested in this and other related modeling for flood risk management.

Data availability. Data are obtained from open sources (https://www.mrlc.gov/viewer/, MRLC, 2023; https://websoilsurvey.nrcs.usda.gov/app/WebSoilSurvey.aspx, USDA – NRCS, 2023) and referenced in the reference list.

Author contributions. BIG, IP, VS, and BB conceptualized and designed the study. BIG did the methodology and draft paper write-up. BIG and IP did the first figure preparations. Improvements, final reviews, and edits were done by IP, VS, and BB. All authors undertook the analysis.

Competing interests. The contact author has declared that none of the authors has any competing interests.

Disclaimer. Publisher's note: Copernicus Publications remains neutral with regard to jurisdictional claims in published maps and institutional affiliations.

Special issue statement. This article is part of the special issue "Advances in pluvial and fluvial flood forecasting and assessment and flood risk management". It is a result of the EGU General Assembly 2022, Vienna, Austria, 23–27 May 2022.

Review statement. This paper was edited by Dhruvesh Patel and reviewed by three anonymous referees.

References

Abbott, M. B., Bathurst, J. C., Cunge, J. A., O'Connell, P. E., and Rasmussen, J.: An introduction to the European Hydrological System – Systeme Hydrologiquee Europeen, "SHE": History and philosophy of a physically-based, distributed modeling system, J. Hydrol., 87, 45–59, https://doi.org/10.1016/0022-1694(86)90114-9, 1986.

Anselmo, V., Galeati, G., Palmieri, S., Rossi, U., and Todini, E.: Flood risk assessment using an integrated hydrological hydraulic modeling approach: a case study, J. Hydrol., 175, 533–554, https://doi.org/10.1016/S0022-1694(96)80023-0, 1996.

Bhatt, C. M., Rao, G. S., Diwakar, P. G., and Dadhwal, V. K.: Development of flood inundation extent libraries over a range of potential flood levels: a practical framework for quick flood response, Geomat. Nat. Haz. Risk, 8, 384–401, https://doi.org/10.1080/19475705.2016.1220025, 2017.

Bhattacharya, B., Mazzoleni, M., and Ugay, R.: Flood inundation mapping of the sparsely gauged large-scale Brahmaputra basin using remote sensing products, Remote Sens., 11, 501, https://doi.org/10.3390/rs11050501, 2019.

Bhusal, A., Parajuli, U., Regmi, S., and Kalra, A.: Application of Machine Learning and Process-Based Models for Rainfall-Runoff Simulation in DuPage River Basin, Illinois, Hydrology, 9, 117, https://doi.org/10.3390/hydrology9070117, 2022.

Brink, E., Aalders, T., Ádám, D., Feller, R., Henselek, Y., Hoffmann, A., Ibe, K., Matthey-Doret, A., Meyer, M., Negrut, N. L., Rau, A. L., Riewerts, B., von Schuckmann, L., Törnros, S., von Wehrden, H., Abson, D. J., and Wamsler, C.: Cascades of green: A review of ecosystem-based adaptation in urban areas, Global Environ. Chang., 36, 111–123, https://doi.org/10.1016/j.gloenvcha.2015.11.003, 2016.

Bronstert, A., Niehoff, D., and Brger, G.: Effects of climate and land-use change on storm runoff generation: Present knowl-

edge and modeling capabilities, Hydrol. Process., 16, 509–529, https://doi.org/10.1002/hyp.326, 2002.

Chen, M., Li, Z., Gao, S., Luo, X., Wing, O. E. J., Shen, X., Gourley, J. J., Kolar, R. L., and Hong, Y.: A comprehensive flood inundation mapping for Hurricane Harvey using an integrated hydrological and hydraulic model, J. Hydrometeorol., 22, 1713–1726, https://doi.org/10.1175/JHM-D-20-0218.1, 2021.

Cohen-Shacham, E., Walters, G., Janzen, C., and Maginnis, S.: Nature-based solutions to address global societal challenges, IUCN International Union for Conservation of Nature, https://doi.org/10.2305/iucn.ch.2016.13.en, 2016.

Dartmouth Flood Observatory: Hurricane Matthew Flooding, Dartmouth Flood Observatory, https://floodobservatory.colorado.edu/Events/2016USA4402/2016USA4402.html (last access: 15 November 2022), 2016.

Dartmouth Flood Observatory: Tropical Storm Florence, Dartmouth Flood Observatory, https://floodobservatory.colorado.edu/Events/4676/2018USA4676.html (last access: November 2022), 2018.

DNR: South Carolina State Climatology Office, DNR, https://www.dnr.sc.gov/climate/sco/ (last access: November 2022), 2021.

Doll, B., Kurki-Fox, J., and Associate, R.: Evaluating the Capacity of Natural Infrastructure for Flood Abatement at the Watershed Scale, Goldsboro, NC, North Carolina Sea Grant, https://ncseagrant.ncsu.edu/ (last access: November 2022), 2020.

Dutta, D., Herath, S., and Musiake, K.: An application of a flood risk analysis system for impact analysis of a flood control plan in a river basin, Hydrol. Process., 20, 1365–1384, https://doi.org/10.1002/hyp.6092, 2006.

Duane, S., Kennedy, A. D., Pendleton, B. J., and Roweth, D.: Hybrid Monte Carlo, Phys. Lett. B, 195, 216–222, https://doi.org/10.1016/0370-2693(87)91197-X, 1987.

Dutta, D., Teng, J., Vaze, J., Lerat, J., Hughes, J., and Marvanek, S.: Storage-based approaches to build floodplain inundation modeling capability in river system models for water resources planning and accounting, J. Hydrol., 504, 12–28, https://doi.org/10.1016/j.jhydrol.2013.09.033, 2013.

Ecologic Institute: Rivers and estuaries – Coastal Management Webguide – RISC KIT, https://coastal-management.eu/coastal-element/rivers-estuaries.html (last access: November 2022), 2019.

Edwards, A.: Pee Dee town struggles to recover from two floods in three years, Carolina News and Reporter, https://carolinanewsandreporter.cic.sc.edu/nichols-special-project/ (last access: November 2022), 2020.

EESI: Nature as Resilient Infrastructure – An Overview of Nature-Based Solutions, Environmental and Energy Study Institute, https://www.eesi.org/papers/view/fact-sheet-nature-as-resilient-infrastructure-an-overview-of-nature-based-solutions (last access: November 2022), 2019.

El Gharamti, M., McCreight, J. L., Noh, S. J., Hoar, T. J., RafieeiNasab, A., and Johnson, B. K.: Ensemble streamflow data assimilation using WRF-Hydro and DART: novel localization and inflation techniques applied to Hurricane Florence flooding, Hydrol. Earth Syst. Sci., 25, 5315–5336, https://doi.org/10.5194/hess-25-5315-2021, 2021.

Emergency Management NC: Lumber River basin flood analysis and mitigation strategies study, Emergency Management NC, https://www.rebuild.nc.gov/media/77/open (last access: November 2022), 2018.

European Commission: Nature-based solutions, NetworkNature, https://networknature.eu/, last access: November 2022.

European Parliament: Directive 2007/60/EC of the European Parliament and of the Council on the assessment and management of flood risks, EUR-Lex, https://eur-lex.europa.eu/legal-content/EN/TXT/?uri=celex:32007L0060 (last access: November 2022), 2017.

Fish, U. S. and Dahl, T. E.: South Carolina's Wetlands: Status and Trends, 1982–1989, FWS (Fish and Wildlife Service), United States, https://www.fws.gov/wetlands/documents/South-Carolinas-Wetlands-Status-and-Trends-1982-1989.pdf (last access: 13 July 2023), 1999.

Grimaldi, S., Schumann, G. J. P., Shokri, A., Walker, J. P., and Pauwels, V. R. N.: Challenges, Opportunities, and Pitfalls for Global Coupled Hydrologic-Hydraulic Modeling of Floods, Water Resour. Res., 55, 5277–5300, https://doi.org/10.1029/2018WR024289, 2019.

Howie, L.: Community Involvement in Flood Mitigation, A Survey-Based Approach in Marion County, SC, Coastal Carolina University Electronic Theses and Dissertations, 122, United States, https://digitalcommons.coastal.edu/etd/122 (last access: 13 July 2023), 2020.

IPCC: Climate Change 2022: Impacts, Adaptation and Vulnerability. Contribution of Working Group II to the Sixth Assessment Report of the Intergovernmental Panel on Climate Change, edited by: Pörtner, H.-O., Roberts, D. C., Tignor, M., Poloczanska, E. S., Mintenbeck, K., Alegría, A., Craig, M., Langsdorf, S., Löschke, S., Möller, V., Okem, A., and Rama, B., Cambridge University Press. Cambridge University Press, Cambridge, UK and New York, NY, USA, 3056 pp., https://doi.org/10.1017/9781009325844, 2022.

IUCN: Nature-based Solutions, International Union for Conservation of Nature, https://www.iucn.org/our-work/nature-based-solutions, last access: November 2022.

Kalantari, Z., Ferreira, C. S. S., Keesstra, S., and Destouni, G.: Nature-based solutions for flood-drought risk mitigation in vulnerable urbanizing parts of East Africa, Current Opinion in Environmental Science & Health, 5, 73–78, https://doi.org/10.1016/j.coesh.2018.06.003, 2018.

Knebl, M. R., Yang, Z.-L., Hutchison K., and Maidment, D. R.: Regional scale flood modeling using NEXRAD rainfall, GIS, and HEC-HMS/RAS: a case study for the San Antonio River Basin Summer 2002 storm event, J. Environ. Manage., 75, 325–336, https://doi.org/10.1016/j.jenvman.2004.11.024, 2005.

Knutson, T.: Global Warming and Hurricanes, NOAA Geophysical Fluid Dynamics Laboratory, https://www.gfdl.noaa.gov/global-warming-and-hurricanes/, last access: November 2022.

Kossin, J. P.: A global slowdown of tropical-cyclone translation speed, Nature, 558, 104–107, https://doi.org/10.1038/s41586-018-0158-3, 2018.

Kumar, P., Debele, S. E., Sahani, J., Rawat, N., Marti-Cardona, B., Alfieri, S. M., Basu, B., Basu, A. S., Bowyer, P., Charizopoulos, N., Gallotti, G., Jaakko, J., Leo, L. S., Loupis, M., Menenti, M., Mickovski, S. B., Mun, S. J., Gonzalez-Ollauri, A., Pfeiffer, J., Pilla, F., Pröll, J., Rutzinger, M., Santo, M. A., Sannigrahi, S., Spyrou, C., Tuomenvirta, H., and Zieher, T.: Nature-based solutions efficiency evaluation against natural hazards: Modeling

methods, advantages, and limitations, Sci. Total Environ., 784, 147058, https://doi.org/10.1016/j.scitotenv.2021.147058, 2021.

Lama, G. F. C., Giovannini, M. R. M., Errico, A., Mirzaei, S., Padulano, R., Chirico, G. B., and Preti, F.: Hydraulic efficiency of green-blue flood control scenarios for vegetated rivers: 1D and 2D unsteady simulations, Water, 13, 2620, https://doi.org/10.3390/w13192620, 2021.

Ly, S., Charles, C., and Degré, A.: Geostatistical interpolation of daily rainfall at catchment scale: the use of several variogram models in the Ourthe and Ambleve catchments, Belgium, Hydrol. Earth Syst. Sci., 15, 2259–2274, https://doi.org/10.5194/hess-15-2259-2011, 2011.

Mishra, S. K. and Singh, V. P.: SCS-CN Method, in: Soil Conservation Service Curve Number (SCS-CN) Methodology, Water Science and Technology Library, vol. 42, Springer, Dordrecht, https://doi.org/10.1007/978-94-017-0147-1_2, 2003.

MRLC: Multi-Reolution Land Characteistics Consortium viewer, Multi-Resolution Land Characteristics (MRLC) Consortium [data set], https://www.mrlc.gov/viewer/, last access: 13 July 2023.

Mubeen, A., Ruangpan, L., Vojinovic, Z., Sanchez Torrez, A., and Plavšić, J.: Planning and Suitability Assessment of Large-scale Nature-based Solutions for Flood-risk Reduction, Water Resour. Manag., 35, 3063–3081, https://doi.org/10.1007/s11269-021-02848-w, 2021.

Muller, C.: How to Save Nichols, SC: A Small Town Lost in the Floods, Woolpert presentation, https://www.seswa.org/assets/Services/Annual-Conference/2020/3%20-%20Muller.pdf (last access: November 2022), 2020.

NASA: Matthew (Atlantic Ocean), NASA, https://www.nasa.gov/feature/goddard/2016/matthew-atlantic-ocean (last access: March 2023), 2016.

Nash, J. E. and Sutcliffe, J. V.: River Flow Forecasting through Conceptual Model. Part 1 – A Discussion of Principles, J. Hydrol., 10, 282–290, https://doi.org/10.1016/0022-1694(70)90255-6, 1970.

National Hurricane Center: Hurricane Florence, National Hurricane Center, https://www.nhc.noaa.gov/archive/2018/al06/al062018.discus.055.shtml (last access: March 2023), 2018.

NOAA: Inland flooding – A hidden danger of tropical cyclones, National Oceanic and Atmospheric Administration, https://www.noaa.gov/stories/inland-flooding-hidden-danger-of-tropical-cyclones (last access: November 2022), 2018.

NOAA: Hurricanes, National Oceanic and Atmospheric Administration, https://www.noaa.gov/education/resource-collections/weather-atmosphere/hurricanes#:~:text=Hurricanes%2C%20known%20generically%20as%20tropical,energy%20from%20warm%20ocean%20waters (last access: November 2022), 2020.

NRCS Kansas: Manning's n Values for Various Land Covers to Use for Dam Breach Analyses, NRCS Kansas, https://rashms.com/wp-content/uploads/2021/01/Mannings-n-values-NLCD-NRCS.pdf (last access: November 2022), 2016.

Phillips R. C., Samadi S. Z., and Meadows M. E.: How extreme was the October 2015 flood in the Carolinas? An assessment of flood frequency analysis and distribution tails, J. Hydrol., 562, 648–663, https://doi.org/10.1016/j.jhydrol.2018.05.035, 2018.

Ruangpan, L., Vojinovic, Z., Di Sabatino, S., Leo, L. S., Capobianco, V., Oen, A. M. P., McClain, M. E., and Lopez-Gunn, E.: Nature-based solutions for hydro-meteorological risk reduction: a state-of-the-art review of the research area, Nat. Hazards Earth Syst. Sci., 20, 243–270, https://doi.org/10.5194/nhess-20-243-2020, 2020.

Sahani, J., Kumar, P., Debele, S., Spyrou, C., Loupis, M., Aragão, L., Porcù, F., Shah, M. A. R., and Di Sabatino, S.: Hydro-meteorological risk assessment methods and management by nature-based solutions, Sci. Total Environ., 696, 133936, https://doi.org/10.1016/j.scitotenv.2019.133936, 2019.

Samadi, S., Pourreza-Bilondi, M., Wilson, C. A. M. E., and Hitchcock, D. B.: Bayesian model averaging with fixed and flexible priors: Theory, concepts, and calibration experiments for rainfall-runoff modeling, J. Adv. Model. Earth Syst., 12, e2019MS001924, https://doi.org/10.1029/2019MS001924, 2020.

SCDNR: Boating Guide to the Little Pee Dee Scenic River Water Trail in Dillon County, South Carolina Department of Natural Resources, South Carolina State Library, http://hdl.handle.net/10827/25678 (last access: November 2022), 2009.

SCDNR: Flood Mitigation Program, South Carolina Department of Natural Resources, https://www.dnr.sc.gov/water/flood/ (last access: November 2022), 2020.

SCS: National Engineering Handbook, Section 4, Soil Conservation Service, U.S. Department of Agriculture, Washington, D.C., https://directives.sc.egov.usda.gov/OpenNonWebContent.aspx?content=18393.wba (last access: 13 July 2023), 1972.

Smith, A. B.: U.S. Billion-dollar Weather and Climate Disasters, 1980–present (NCEI Accession 0209268), NOAA National Centers for Environmental Information [data set], https://doi.org/10.25921/stkw-7w73, 2020.

Soulis, K. X.: Soil Conservation Service Curve Number (SCS-CN) Method: Current Applications, Remaining Challenges, and Future Perspectives, Water, 13, 192, https://doi.org/10.3390/w13020192, 2021.

Stewart, S. R. and Berg, R.: Hurricane Florence, National Hurricane Center, Tropical Cyclone Report, https://www.nhc.noaa.gov/data/tcr/AL062018_Florence.pdf (last access: 13 July 2023), 2019.

Stone, M. H. and Cohen, S.: The influence of an extended Atlantic hurricane season on inland flooding potential in the southeastern United States, Nat. Hazards Earth Syst. Sci., 17, 439–447, https://doi.org/10.5194/nhess-17-439-2017, 2017.

Tang, Y., Leon, A. S., and Kavvas, M. L.: Impact of Size and Location of Wetlands on Watershed-Scale Flood Control, Water Resour. Manag., 34, 1693–1707, https://doi.org/10.1007/s11269-020-02518-3, 2020.

Tedesco, M., McAlpine, S., and Porter, J. R.: Exposure of real estate properties to the 2018 Hurricane Florence flooding, Nat. Hazards Earth Syst. Sci., 20, 907–920, https://doi.org/10.5194/nhess-20-907-2020, 2020.

Teng, J., Jakeman, A. J., Vaze, J., Croke, B. F. W., Dutta, D., and Kim, S.: Flood inundation modeling: A review of methods, recent advances, and uncertainty analysis, Environ. Model. Softw., 90, 201–216, https://doi.org/10.1016/j.envsoft.2017.01.006, 2017.

Thomas, H. and Nisbet, T. R.: An assessment of the impact of floodplain woodland on flood flows, Water Environ. J., 21, 114–126, https://doi.org/10.1111/j.1747-6593.2006.00056.x, 2007.

US Army Corps of Engineers: HEC-RAS River Analysis System Hydraulic Reference Manual, Version 5.0, US Army Corps of Engineers, https://www.hec.usace.army.mil/software/hec-ras/documentation/HEC-RAS%205.0%20Reference%20Manual.pdf (last access: 13 July 2023), 2016.

US Army Corps of Engineers: Hydrologic Modeling System HEC-HMS Technical Reference Manual CPD-74B, US Army Corps of Engineers, https://www.hec.usace.army.mil/software/hec-hms/documentation/HEC-HMS_Technical%20Reference%20Manual_(CPD-74B).pdf (last access: 13 July 2023), 2021.

USDA – NRCS: Web Soil Survey, U.S. Department of Agriculture (USDA) [data set], https://websoilsurvey.nrcs.usda.gov/app/WebSoilSurvey.aspx, last access: 13 July 2023.

USGS: National Water Information System, United States Geological Survey, https://waterdata.usgs.gov/nwis (last access: 13 July 2023), 2023.

Williams, T., Song, B., Hitchcock, B., and O'Halloran, T.: Hurricane Florence Flooding in Georgetown County: A Qualitative Explanation of the Interactions of Estuary and Tidal River, Journal of South Carolina Water Resources, 6, 35–49, https://doi.org/10.34068/JSCWR.06.04, 2019.

Williams, T., Song, B., Hitchcock, B., and O'Halloran, T.: Floodplain Geomorphology and Response to Hurricanes: Lower Pee Dee Basin, South Carolina. Journal of South Carolina Water Resources, 7, 81–90, https://doi.org/10.34068/JSCWR.07.06, 2020.

Wing, O. E. J., Sampson, C. C., Bates, P. D., Quinn, N., Smith, A. M., and Neal, J. C.: A flood inundation forecast of Hurricane Harvey using a continental-scale 2D hydrodynamic model, J. Hydrol., 4, 100039, https://doi.org/10.1016/j.hydroa.2019.100039, 2019.

Zhou, X., Ma, W., Echizenya, W., and Yamazaki, D.: The uncertainty of flood frequency analyses in hydrodynamic model simulations, Nat. Hazards Earth Syst. Sci., 21, 1071–1085, https://doi.org/10.5194/nhess-21-1071-2021, 2021.